Materials & Design 227 (2023) 111709

Contents lists available at ScienceDirect

Materials & Design

journal homepage: www.elsevier.com/locate/matdes

Single-phase lightweight high-entropy alloys with enhanced mechanical properties

Il-Seok Jeong, Joo-Hyoung Lee *

School of Materials Science and Engineering, Gwangju Institute of Science and Technology, Gwangju 61005, Republic of Korea

GRAPHICAL ABSTRACT

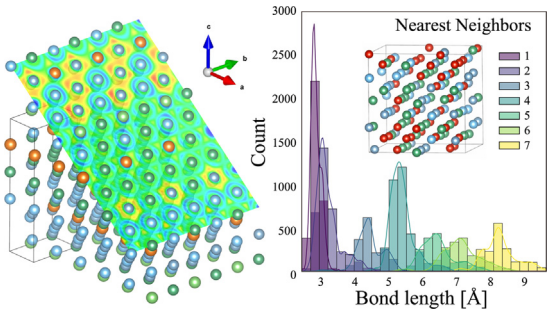

ARTICLE INFO

Article history:
Received 29 November 2022
Revised 5 February 2023
Accepted 5 February 2023
Available online 7 February 2023

Keywords:
High-entropy alloys
Lightweight
Density Functional Theory
Ductility

ABSTRACT

To develop single-phase lightweight high-entropy alloys (LWHEAs), we perform massive screening over a vast material space containing more than 560,000 possible compounds by employing thermodynamic principles and examine the mechanical properties of the resulting alloys based on density functional theory (DFT) calculations. Considering LWHEAs composed of five principal elements including light atoms such as Li, Mg and Al, we identify 40 optimal atomic compositions for single-phase solid solutions in body-centered-cubic structure. Combined with DFT calculations, it is demonstrated that the valence electron concentration plays an important role in determining elastic moduli and that the identified LWHEAs are ductile as is evidenced by the satisfied Pugh criteria and positive Cauchy pressure. In cases of shear modulus and yield strength, *pd*-hybridization between Al and transition metal atoms is shown to make a significant contribution through forming strong directional bonds. Together with an observation that the inclusion of Li and Mg atoms is instrumental in reducing the overall density, the present results provide a valuable guidance to develop novel, low-density high-entropy alloys.

1. Introduction

The demand for lightweight (LW) materials is higher than ever due to the increasing need for applications such as in automotive, aviation and other transportation sectors where energy efficiency and reduction of carbon dioxide emissions are becoming a critical issue [1–5]. Efforts to achieve high-performance LW materials for targeted applications have been attempted predominantly through alloying approaches. In traditional alloying schemes, small amounts of secondary elements are incorporated into a host material to improve materials' properties, which has been successfully utilized for centuries. Relatively recently, however, a novel alloying strategy based on multiple principal elements was introduced, which opened up a unique avenue for developing a vast number of advanced materials [6,7].

* Corresponding author.
E-mail address: jhyoung@gist.ac.kr (J.-H. Lee).

https://doi.org/10.1016/j.matdes.2023.111709
0264-1275/

These new alloys, referred to as high entropy alloys (HEAs), have high configurational entropy due to a nearly equal-atomic-ratio composition of five or more major elements, which avoids the formation of intermetallic (IM) compounds and results in stabilization into simple solid solution phases [8]. In fact, special interest in high entropy alloys stems from the fact that HEAs composed of multiple transition metal (TM) elements have demonstrated superior performance such as high resistance against corrosion [9], wear [10] and oxidation [11] together with excellent mechanical properties at various temperatures [12–14]. Inspired by these advancements, much effort has been made to extend the high entropy alloying scheme to incorporate light elements such as Li, Mg and Al, which has resulted in lightweight high entropy alloys (LWHEAs) [15].

The density of LWHEAs is primarily determined by the amount of light elements such as Al, Li and Mg, leading to an overall density ranging from 2.67 g cm^{-3} to 6.09 g cm^{-3} [16–18]. However, unlike conventional HEAs that are stabilized in single-phase solid solutions such as body-centered-cubic (BCC) or face-centered-cubic (FCC) phases, LWHEAs reported so far have exhibited diverse structural complexities including mixed phase states and intermetallics as well as single phase structures. For instance, FCC Al-Li-Mg-Sc-Ti alloys were synthesized through mechanical alloying, which is transformed to a HCP structure when sintered [16]. The strong interaction between Al/Ti and 3*d* TM metals readily forms IM compounds [19], and the microstructures of Li- and Mg-containing LWHEAs showed a mixture of different IM compounds [17]. Such multi-phase structures present a major challenge for applications of LWHEAs because the resulting alloys are likely to exhibit high level of brittleness, which could be circumvented through constructing single-phase LWHEAs.

It should be admitted, however, that developing single-phase LWHEAs with minimized brittleness is a highly convoluted multivariate optimization problem because both the selection of constituent elements and their atomic fraction should be carefully regulated. To tackle this issue, we employ combined thermodynamic principles and ab-initio computational approaches and carry out massive screening over a large-scale material space. The formability of a single phase LWHEA is assessed through thermodynamics parameters, and the resulting compounds are systematically examined for structural and mechanical properties based on first-principles electronic structure calculations. Careful investigation of the screened LWHEAs demonstrates that the absence of *p*-orbitals in Li and Mg gives rise to different bonding characteristics with neighboring TM elements compared to Al, which then brings about contrasting effects on mechanical properties of LWHEAs. These results not only shed a new light on the role of light elements other than Al in determining physical properties of high entropy alloys but also provide a valuable guidance to develop novel LWHEAs for applications where enhanced performance is highly desired together with reduced weights.

2. Computational methods

Screening for single phase structures. To evaluate the formability of solid solution (SS) phases of multicomponent alloys, the phase formation rules dictated by the thermodynamic parameters (Table 1) are employed. In order to facilitate the formation of SS phases, small values of both atomic size (δ) and electronegativity differences ($\Delta\chi$), near zero values of mixing enthalpy (ΔH_{mix}) and large entropy-to-enthalpy ratios (Ω) are needed as well as high mixing entropy (ΔS_{mix}) [17]. In cases of conventional HEAs that are mainly composed of TM elements, the criteria for forming SS phases are given as $-15 < \Delta H_{mix} < 5$ kJ/mol [20], $\delta < 5\%$, $\Omega \geq 1.1$ and $\delta < 6.6\%$ [21], respectively. However, light elements lacking *d* orbitals such as Li, Mg, and Al favor the formation of ordered compounds rather than disordered solid solutions. This observation makes the phase formation rules for low-density multi-element alloys more strict than those for conventional HEAs, which leads to the following screening criteria: $-1 < \Delta H_{mix} \leq 5$kJ/mol, $\Omega > 10$, $\delta < 4.5\%$ and $\Delta x < 0.175$ [17].

Table 1
Thermodynamic and physical parameters for phase formation rules of HEAs. c_i is the atomic percentage of the *i*-th element, R the ideal gas constant, and ΔH_{ij}^{mix} the enthalpy of mixing of binary alloys, respectively. $(T_m)_i$, χ_i, $(\mathrm{VEC})_i$, A_i, and ρ_i are the melting temperature, Pauling electronegativity, valence electron concentration, atomic weight and density of the *i*-th element, respectively.

Parameter	Definition	Formula
ΔS_{mix}[Jmol^{-1}K^{-1}]	Entropy of mixing	$\Delta S_{mix} = -R\sum_{i=1}^{N}(c_i \ln c_i)$
ΔH_{mix}[kJmol^{-1}]	Enthalpy of mixing	$\Delta H_{mix} = \sum_{i=1, i\neq j}^{N} 4c_i c_j \Delta H_{ij}^{mix}$
δ [%]	Atomic size difference	$\delta = 100\%\sqrt{\sum_{i=1}^{N} c_i\left(r_i/\sum_{j=1}^{N} c_j r_j\right)^2}$
T_m [K]	Theoretical melting temperature	$T_m = \sum_{i=1}^{N} c_i (T_m)_i$
Ω	Ratio of entropy to enthalpy values	$\Omega = \frac{T_m \Delta S_{mix}}{\lvert\Delta H_{mix}\rvert}$
$\Delta\chi$	Electronegativity difference	$\Delta\chi = \sqrt{\sum_{i=1}^{N} c_i\left(\chi_i - \sum_{j=1}^{N} c_j \chi_j\right)^2}$
VEC	Valence electron concentration	$\mathrm{VEC} = \sum_{i=1}^{N} c_i (\mathrm{VEC})_i$
ρ [g cm^{-3}]	Theoretical density	$\rho = \frac{\sum_{i=1}^{N} c_i A_i}{\sum_{i=1}^{N} c_i A_i/\rho_i}$

First-principles calculations. To investigate mechanical properties of LWHEAs, we carry out density functional theory (DFT) calculations by employing Vienna Ab-initio Simulation Package (VASP) [22]. The Kohn-Sham equation is solved based on plane-wave basis of 400 eV cutoff together with projector augmented wave (PAW) [23] method, and exchange–correlation interaction among electrons is treated within generalized gradient approximation (GGA) [24]. To perform integration over the first Brillouin zone, $3 \times 3 \times 2$ **k**-meshes are utilized for both structural optimization and calculation of elastic properties. To examine the bonding characteristics between atoms in LWHEAs, we perform detailed analyses based on the electron localization function (ELF) [25], density derived electrostatic and chemical (DDEC6) method [26] and crystal overlap Hamilton population (COHP) [27] approaches. It should be noted that due to the high-entropic nature of the alloys, it is necessary to take random structure into account. To address this issue, we employ special quasi-random structure (SQS) [28] method as is implemented in ATAT package [29] and generate LWHEA supercells which are composed of $3 \times 4 \times 5$ conventional BCC units containing 120 atoms.

3. Results and discussion

3.1. Alloy screening and structural properties

To perform screening for novel LWHEAs, we begin with the following 11 elements which are commonly studied in producing lightweight alloys: Li, Mg, Al, Ti, V, Nb, Zr, Hf, Mo, W and Ta. To construct quinary LWHEAs, 5 elements out of 11 elements are selected with the atomic fraction of each constituent lying between 5 % and 35 %, which results in an extensive material space containing more than 560,000 possible combinations. In screening over these materials, it should be noted that valence electron concentration (VEC) plays an important role in the phase stability of HEAs in addition to the aforementioned thermodynamic parameters. For VEC greater than 8, FCC solid solution is stabilized, whereas BCC solid solution is favored when VEC is smaller than 6.87, and solid solution of mixed FCC and BCC phases is formed

with $6.87 \leq VEC \leq 8$ [30]. Investigating all the possible compounds for the formation of stable solid solutions based on the thermodynamic parameters as well as VEC, it is found that 80 candidate materials are expected to form BCC phase with density lower than 6 g/cm^3 to be considered as lightweight alloys [19].

However, it should be noted that the high reactivity of the low-density elements with the environment becomes one of the major challenges in synthesizing LWHEAs [15]. In particular, the presence of a high fraction of high vapor pressure elements such as Li, Mg, Zn, and Mn makes melt-synthesis difficult, so it is necessary to reduce the content of these elements as low as possible [31]. In the present study, we follow previous studies and keep a total atomic weight of Li and Mg less than 10 % [31,32] of the entire unit cell, which finally enables us to identify 40 alloys in BCC structure for LWHEAs (Table 2). The resulting LWHEAs are further divided into three groups according to the light elements contained in the compounds: Li-Mg-Al-X-Y (12), Li-Al-X-Y-Z (6), and Mg-Al-X-Y-Z (22). Here, X, Y, and Z are transition metal elements (Ti, V, Zr, Nb, Hf, Ta, Mo, and W), and numbers in parentheses indicate the number of alloys in each group. The obtained LWHEAs are plotted in terms of δ and ΔH_{mix} in Fig. 1(a) and with respect to $\Delta\chi$ and Ω in Fig. 1(b), respectively. As is seen from the figures, while the criteria for thermodynamic parameters predict the stabilization in BCC structures of the above LWHEAs, the same criteria also well describe the formation of stable solid solution phases of other high entropy alloys such as refractory HEAs or existing LWHEAs [19].

Fig. 1(c) shows the lattice parameters (a) of optimized LWHEAs as a function of valence electron concentration. As is presented in Fig. 1(c), the average lattice constant a of a conventional cubic unit is 3.33 Å, showing a linear decrease with VEC. It is further found that a of LWHEAs containing Li and Al is shorter (3.23 Å) than those of Li-Mg-Al-X-Y (3.31 Å) and Mg-Al-X-Y-Z (3.37 Å) alloys, which makes the density of Li-Al-X-Y-Z highest (5.79 g/cm^3). In contrast, Li-Mg-Al-X-Y shows the lowest density (5.20 g/cm^3), leading to the overall density of 5.49 g/cm^3 for the proposed LWHEAs.

3.2. Mechanical properties

Elastic modulus. In studying mechanical properties of LWHEAs, we first calculate the elastic moduli including bulk modulus B and shear modulus G. To this end, the elastic constants, C_{ij}, are obtained from the total energy calculations with infinitesimal deformation introduced into a unit cell, and the elastic moduli are then obtained by inverting the stiffness tensor. Fig. 2(a) shows the obtained bulk modulus, and as is clearly seen in the figure, B displays a strong linear increase as a function of VEC. Such linear dependence of B is understood by noting that bulk modulus measures volumetric resistance of a material against compressive deformation, and high VEC implies enhanced repulsive response upon compression, thus leading to high B values [33]. In contrast, the shear modulus does not show a comprehensible relation with VEC in that G is distributed over a wide range of VEC with the average of 25.9 GPa

Table 2
List of LWHEAs. A complete list of screened LWHEAs together with parameters for the phase formation rules. The numbers in subscript represent the atomic percentage.

HEAs	ΔS_{mix}	ΔH_{mix}	VEC	δ	Ω	$\Delta\chi$	ρ
$Li_{05}Al_{20}Mg_{10}Ti_{30}Nb_{35}$	11.9	0.3	3.8	3.5	76	0.152	5.0
$Li_{05}Al_{20}Mg_{10}Ti_{35}Nb_{30}$	11.9	−0.7	3.8	3.5	32	0.151	4.8
$Li_{05}Al_{20}Mg_{15}Ti_{35}Nb_{25}$	12.2	1.4	3.6	4.0	15	0.156	4.4
$Li_{05}Al_{25}Mg_{15}Ti_{20}Nb_{35}$	12.2	1.3	3.7	4.1	16	0.160	4.7
$Li_{05}Al_{25}Mg_{15}Ti_{25}Nb_{30}$	12.4	0.1	3.6	4.1	176	0.159	4.5
$Li_{05}Al_{30}Mg_{15}Ti_{15}Nb_{35}$	12.0	−0.4	3.6	4.2	52	0.161	4.7
$Li_{05}Al_{15}Mg_{25}Ti_{30}Hf_{25}$	12.4	−0.8	3.2	4.5	24	0.161	5.7
$Li_{05}Al_{20}Mg_{20}Ti_{35}Ta_{20}$	12.3	1.9	3.5	4.3	11	0.151	5.6
$Li_{05}Al_{25}Mg_{20}Ti_{30}Ta_{20}$	12.5	−0.6	3.4	4.4	37	0.154	5.5
$Li_{10}Al_{10}Mg_{25}Zr_{35}Hf_{20}$	12.4	0.6	3.1	3.4	31	0.142	5.8
$Li_{15}Al_{15}Mg_{25}Zr_{15}Hf_{30}$	13.0	0.1	2.9	3.8	218	0.173	6.0
$Li_{15}Al_{15}Mg_{25}Zr_{20}Hf_{25}$	13.2	−0.3	2.9	3.8	56	0.173	5.7
$Li_{05}Al_{10}Ti_{25}V_{25}Nb_{35}$	12.0	−0.2	4.4	4.3	110	0.138	5.9
$Li_{05}Al_{10}Ti_{30}V_{20}Nb_{35}$	11.9	−0.3	4.3	4.0	80	0.137	5.8
$Li_{05}Al_{10}Ti_{30}V_{25}Nb_{30}$	12.0	−0.7	4.3	4.3	37	0.137	5.7
$Li_{05}Al_{10}Ti_{35}V_{15}Nb_{35}$	11.6	−0.4	4.3	3.6	69	0.136	5.8
$Li_{05}Al_{10}Ti_{35}V_{20}Nb_{30}$	11.9	−0.8	4.3	4.0	32	0.137	5.6
$Li_{05}Al_{10}Ti_{35}Zr_{15}Nb_{35}$	11.6	−0.9	4.1	4.0	28	0.152	5.9
$Al_{10}Mg_{10}Ti_{35}Zr_{10}Nb_{35}$	11.9	−0.1	4.1	4.4	403	0.106	5.6
$Al_{15}Mg_{15}Ti_{30}Zr_{05}Nb_{35}$	12.0	0.2	3.9	4.4	106	0.109	5.2
$Al_{15}Mg_{15}Ti_{35}Zr_{05}Nb_{30}$	12.0	−0.7	3.9	4.4	34	0.108	5.0
$Al_{05}Mg_{20}Ti_{25}Zr_{35}Hf_{15}$	12.2	0.3	3.6	4.2	90	0.109	6.0
$Al_{05}Mg_{20}Ti_{30}Zr_{30}Hf_{15}$	12.3	0.8	3.6	4.3	28	0.113	5.9
$Al_{05}Mg_{20}Ti_{35}Zr_{25}Hf_{15}$	12.2	1.3	3.6	4.4	17	0.115	5.8
$Al_{05}Mg_{25}Ti_{20}Zr_{35}Hf_{15}$	12.2	1.3	3.5	4.0	17	0.104	5.8
$Al_{05}Mg_{25}Ti_{25}Zr_{30}Hf_{15}$	12.4	1.9	3.5	4.2	12	0.109	5.7
$Al_{05}Mg_{30}Ti_{15}Zr_{35}Hf_{15}$	12.0	1.9	3.4	3.7	11	0.098	5.6
$Al_{10}Mg_{30}Ti_{25}Zr_{10}Hf_{25}$	12.6	−0.4	3.3	4.4	56	0.121	6.0
$Al_{10}Mg_{30}Ti_{30}Zr_{05}Hf_{25}$	12.0	0.5	3.3	4.4	41	0.124	5.9
$Al_{15}Mg_{15}Ti_{30}Nb_{35}Mo_{05}$	12.0	1.4	4.0	4.3	18	0.168	5.4
$Al_{15}Mg_{15}Ti_{35}Nb_{30}Mo_{05}$	12.0	0.5	4.0	4.2	44	0.168	5.2
$Al_{15}Mg_{15}Ti_{30}Nb_{35}Hf_{05}$	12.0	0.5	3.9	4.3	48	0.112	5.6
$Al_{15}Mg_{15}Ti_{35}Nb_{30}Hf_{05}$	12.0	−0.4	3.9	4.2	59	0.111	5.5
$Al_{15}Mg_{15}Ti_{30}Nb_{35}Ta_{05}$	12.0	1.5	4.0	4.0	16	0.100	5.7
$Al_{15}Mg_{15}Ti_{35}Nb_{30}Ta_{05}$	12.0	0.6	3.9	4.0	37	0.099	5.5
$Al_{20}Mg_{20}Ti_{25}Nb_{25}Ta_{10}$	13.0	1.2	3.8	4.5	21	0.110	5.7
$Al_{20}Mg_{20}Ti_{25}Nb_{30}Ta_{05}$	12.5	1.3	3.8	4.5	17	0.112	5.3
$Al_{20}Mg_{20}Ti_{30}Nb_{25}Ta_{05}$	12.5	0.2	3.7	4.4	102	0.110	5.1
$Al_{20}Mg_{20}Ti_{35}Nb_{20}Ta_{05}$	12.3	−0.9	3.7	4.4	23	0.109	4.9
$Al_{10}Mg_{30}Ti_{35}Zr_{10}Hf_{15}$	12.3	−0.5	3.4	4.3	43	0.116	5.9

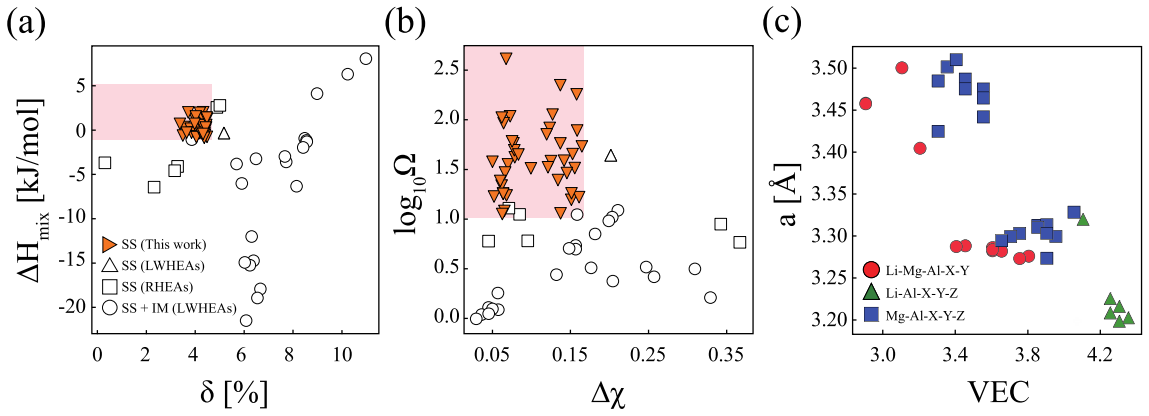

Fig. 1. Screening results for LWHEAs. (a) Atomic size difference (δ) versus enthalpy of mixing. (b) Pauling electronegativity difference versus $\log_{10}\Omega$. The shaded areas represent the region of solid solution (SS) phases. (c) The calculated lattice constants *a* as a function of VEC.

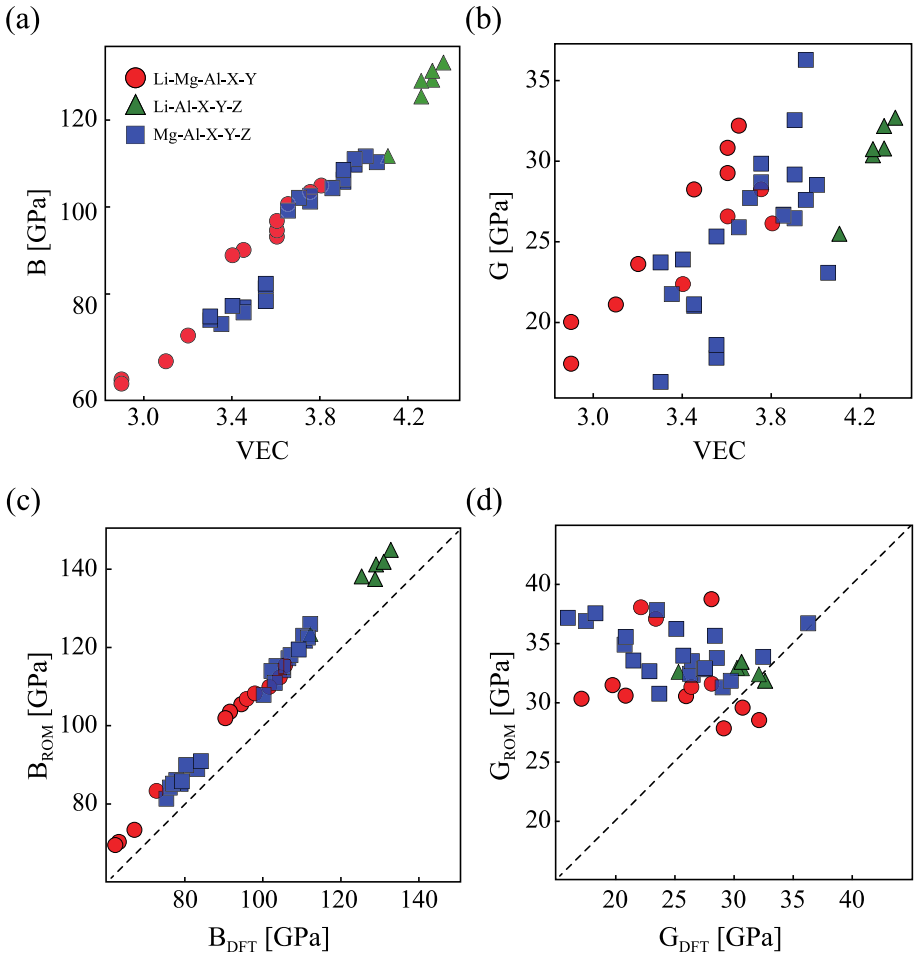

Fig. 2. Elastic moduli of LWHEAs. (a) bulk modulus *B*, (b) shear modulus *G* as a function of VEC. Comparison between DFT- (X_{DFT}) and ROM-calculated (X_{ROM}) values (X = *B* or *G*): (c) bulk modulus and (d) shear modulus, respectively.

(Fig. 2(b)). It is noted that Mg-Al alloys exhibits a wider variation in *G* than the other two cases with 16 and 36 GPa for minimum and maximum values, respectively.

When computing mechanical properties of conventional HEAs, the rule of mixture (ROM) [14] has been commonly applied. In the ROM, a given physical property *M* of HEAs is calculated from $M = \sum_i c_i M_i$, where c_i is the atomic fraction and M_i the corresponding property of the *i*-th constituent, respectively. In Fig. 2(c) and 2 (d), the DFT-computed values of *B* and *G* are presented against those obtained from the ROM. As is evident from Fig. 2(c), the DFT results present good agreement with the ROM values for bulk modulus. On the other hand, however, the difference in shear modulus between the DFT and ROM values is striking (Fig. 2(d)) in that the results from the ROM are confined within a rather narrow range with 33 GPa on average whereas the DFT results range from 16 to 36 GPa. It should be stressed that unlike the present cases,

the ROM values of shear modulus exhibit close agreement with those from DFT calculations for other high entropy alloys.

To gain an insight into the contrasting results of the DFT and ROM calculations regarding bulk and shear moduli, we plot the DFT-computed G with respect to the average number of Al and average number of Li and Mg in the nearest neighbor of TM elements in Fig. 3(a). As is clear from Fig. 3(a), the G values become higher when more Al are present around TM elements whereas large amount of Li and Mg tends to reduce the shear modulus. Such difference can be understood from disparate bonding characteristics between component atoms within LWHEAs. Fig. 3(b) shows an electron localization function (ELF) of a Li-Mg-Al-Ti-Nb alloy, projected on (101) plane. We note that similar ELF is also observed in other cases. Evidently, the ELF around Al has higher values than those around Li, Mg or TM elements, which indicates that the bonding nature between Al and TM is different from all the other cases. In conventional HEAs that are composed of multiple TM elements, the ELF are found to have values close to the ones around TM atoms in the present cases, suggesting that all bonds are of the same type (non-directional metallic bonds) [34]. However, the high ELF values around Al implies the formation of directional covalent bonds with TM atoms through *pd* hybridization, which exhibits strong resistance to shear deformation [35,36].

Fig. 3(c) presents the bond orders (BOs) for all atom pairs in 40 LWHEAs, calculated with DDEC6. It is seen from the figure that the BOs of Li- and Mg-containing bonds are definitely lower than those of Al-Al, Al-TM and TM-TM bonds. Also, the BO of Al-Al or Al-TM is distributed over the nearly same range of TM-TM cases, which suggests that the Al-TM bonds are likely to be as strong as the bonds between transition metal elements. Accumulated electrons on the Al-TM bonds, together with high level of the bonding state as is evidenced by the large negative values of the integrated COHP (-ICOHP), substantially contributes to enhancing the shear modulus.

Ductility. The intrinsic ductility is an important characteristic for practical application of materials. While it is extremely challenging to compute ductility from first-principles, the Cauchy pressure $\bar{C}_{12} - \bar{C}_{44}$, where $\bar{C}_{12} = (C_{12} + C_{23} + C_{13})/3$ and $\bar{C}_{44} = (C_{44} + C_{55} + C_{66})/3$, respectively, has been utilized as a valuable metric to estimate the deformability of materials for gauging ductility. It is known that the Cauchy pressure holds a close relation with angular character of atomic bonding, that is, positive and negative

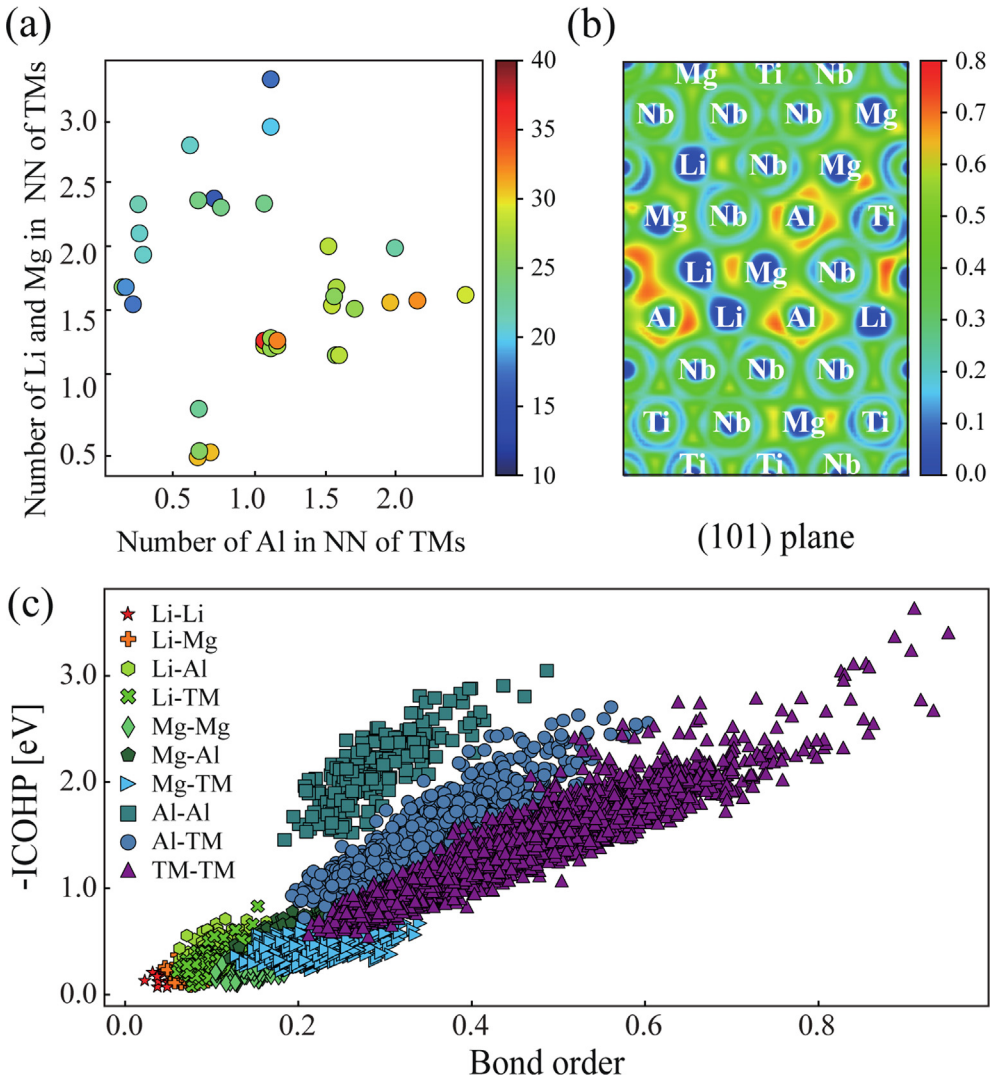

Fig. 3. (a) Distribution of shear modulus of 40 screened LWHEAs as a function of average number of Al (x-axis), Li and Mg (y-axis) in the nearest neighbor (NN) of TM elements. The shear modulus is displayed by the colored circles with the color scale on the right. (b) Contour map of the electron localization function of $Li_5Mg_{10}Al_{20}Ti_{30}Nb_{35}$. The ELF map is projected onto (101) plane and the color scale is presented on the right. (c) Distribution of the atomic bonds within LWHEAs with respect to bond order (x-axis) and -ICOHP (y-axis).

Cauchy pressure correspond to non-directional and covalent, directional bonding, respectively. In Fig. 4(a), ductility of the present LWHEAs is examined based on the widely used criteria by Pugh [37] and Pettifor [38], respectively. Interestingly, there exists an apparent linear relation between the G/B ratio and Cauchy pressure rescaled by bulk modulus ($(\bar{C}_{12}-\bar{C}_{44})/B$). It is seen from Fig. 4 (a) that the G/B values of all LWHEAs are smaller than the critical value (dotted, vertical line in the figure), implying that all the proposed LWHEAs in the present study are ductile. Besides, the Pettifor criterion for ductile behavior is also satisfied as is seen from the positivity of $(\bar{C}_{12}-\bar{C}_{44})/B$. The ductile behavior originates from the non-directional bonding between TM atoms and between Li or Mg and TM atoms which compensates for the strong directionality in Al-TM bonding. In Fig. 4(b), the rescaled Cauchy pressure is plotted against VEC. As is seen from the figure, $(\bar{C}_{12}-\bar{C}_{44})/B$ exhibits an overall linear increase with VEC, which holds the highest and lowest values for Li-Al-X-Y-Z and Li-Mg-Al-X-Y alloys, respectively. The observed linear dependence demonstrates that ductility can be systematically tuned by modulating the types and amounts of light elements as well as amount of Al just as in other mechanical properties.

Yield strength. Yield strength (σ_Y) makes an important mechanical property in designing high-performance alloys and their applications. In the present study, the yield strength of LWHEAs is evaluated based on the solid solution strengthening as is proposed by Senkov *et al.*[14] and Yao *et al.*[39] In this approach, σ_Y is computed as $\sigma_Y=\sigma_Y^{mix}+\Delta\sigma$ with σ_Y^{mix} being the average yield strength according to the elemental fractions in LWHEAs. $\Delta\sigma$ represents the contribution from the solid solution strengthening, which is obtained by summing up the constituent's values: $\Delta\sigma=\left[\sum_i (AG)^{3/2}\left(\delta_{G_i}^2+\alpha^2\delta_{r_i}^2\right)c_i\right]^{2/3}$. Here, A and α are material-dependent parameters taken from literature [14,39] and G is the DFT-computed shear modulus of LWHEAs, respectively. In the equation for $\Delta\sigma$, δ_{G_i} and δ_{r_i} are defined as $\delta_{G_i}=\sum_j 9(G_i-G_j)/4(G_i+G_j)$ and $\delta_{r_i}=\sum_j 9(r_i-r_j)/4(r_i+r_j)$, respectively, where G_i is the shear modulus of the i-th element.

Fig. 5(a) shows the computed yield strength of the present LWHEAs, and as is seen from the figure Li-Al-X-Y-Z and Li-Mg-

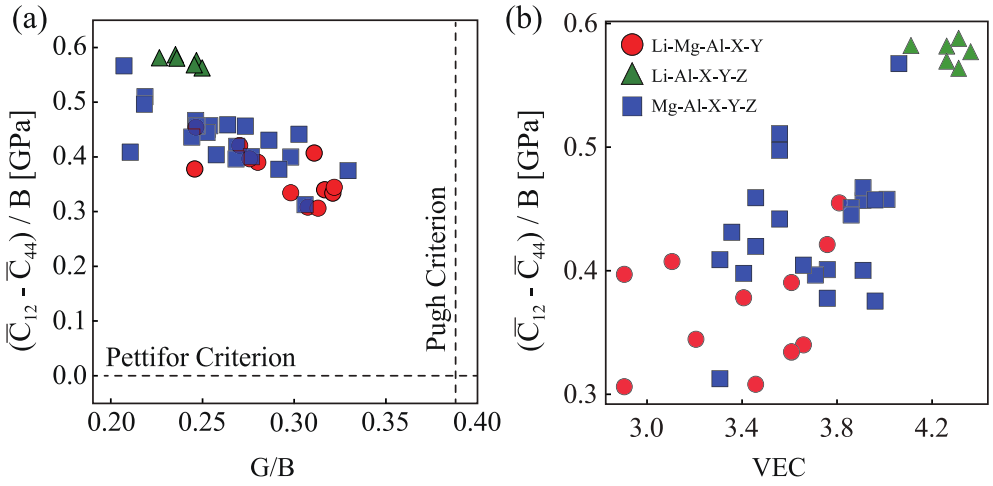

Fig. 4. Ductility of LWHEAs. (a) Distribution of LWHEAs with respect to G/B values (x-axis) and Cauchy pressure rescaled by bulk modulus (y-axis), and (b) B-rescaled Cauchy pressure as a function of VEC.

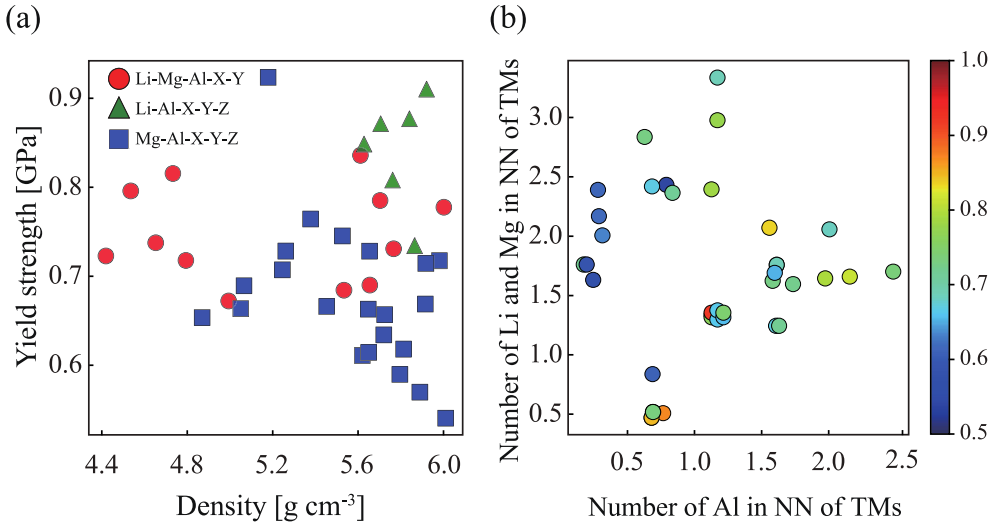

Fig. 5. (a) Yield strength of LWHEAs as a function of density, (b) distribution of yield strength of LWHEAs as a function of average number of Al (x-axis), Li and Mg (y-axis) in the nearest neighbor (NN) of TM elements. The yield strength is displayed by the colored circles with the color scale on the right.

Al-X-Y alloys have a similar range for the yield strength: 0.73 GPa $\leq \sigma_Y \leq$ 0.91 GPa for Li-Al-X-Y-Z and 0.67 GPa $\leq \sigma_Y \leq$ 0.83 GPa for Li-Al-Mg-X-Y, respectively. In contrast, Mg-Al-X-Y-Z alloys show a wider variation in σ_Y ranging from 0.54 to 0.92 GPa. While a random nature of atomic distribution within BCC lattices of LWHEAs makes a thorough analysis of σ_Y between different alloy groups extremely challenging, a clear tendency in σ_Y is observed when the yield strength is plotted against the average number of Al and other lightweight atoms in the nearest neighbor of TM elements. As is seen from Fig. 5(b), σ_Y shows higher values ($\geq$0.65 GPa) when more Al atoms are present around TM elements, whereas no consistent change in σ_Y is witnessed for varying the amount of Li and Mg. Such pronounced dependence of σ_Y on Al is attributed to the formation of strong directional bonds between Al-*p* and TM-*d* orbitals, which also plays a significant role in determining shear modulus in HEAs.

4. Conclusions

Developing novel lightweight high-entropy alloys is a non-trivial task due to a complex multivariate nature arising from simultaneous optimization of atomic species and composition. Such highly combinatorial problems can greatly benefit from computational approaches which enable expedited screening over a vast material space containing all allowed compounds. Indeed, a recent study based on a combined machine-learning and DFT calculation have made it possible to identify new Invar high-entropy alloys with low thermal expansion coefficients.[40] The present study presents an alternative computational route towards a multicomponent optimization problem by employing the solid-solution phase formation rules which are based on thermodynamic parameters. It should be noted that this approach is particularly devised for high-entropy alloys and thus can substantially accelerate the screening procedure without training of algorithms. The resulting LWHEAs possess robust mechanical and ductile properties as is demonstrated with DFT calculations, which makes the new LWHEAs highly appealing for technical applications where energy efficiency is a key issue. It is thus expected that the present results will be a valuable guide to experimental synthesis of novel low-density high-entropy alloys.

Data availability

Data will be made available on request.

Declaration of Competing Interest

The authors declare that they have no known competing financial interests or personal relationships that could have appeared to influence the work reported in this paper.

Acknowledgements

This work was supported by the National Research Foundation (NRF) of Korea grant funded by the Korean Government (NRF-2020R1I1A2074957 and NRF-2020R1A4A1019266).

References

[1] V. Kumar, A. Gupta, D. Lahiri, K. Balani, Serrated yielding during nanoindentation of thermomechanically processed novel Mg-9Li-7Al-1Sn and Mg-9Li-5Al-3Sn-1Zn alloys, J. Phys. D. Appl. Phys. 46 (2013).
[2] V. Kumar, Govind, R. Shekhar, R. Balasubramaniam, K. Balani, Microstructure evolution and texture development in thermomechanically processed Mg–Li–Al based alloys. *Mater. Sci. Eng. A* **547**, 2012 38–50
[3] A. Devaraj et al., A low-cost hierarchical nanostructured beta-titanium alloy with high strength, Nat. Commun. 7 (2016) 11176.
[4] G. Chen et al., Polysynthetic twinned TiAl single crystals for high-temperature applications, Nat. Mater. 15 (2016) 876–881.
[5] L.W. Cheah, J.B. Heywood, Cars on a diet: the material and energy impacts of passenger vehicle weight reduction in the U.S, Massachusetts Institute of Technol. (2010).
[6] B. Cantor, I.T.H. Chang, P. Knight, A.J.B. Vincent, Microstructural development in equiatomic multicomponent alloys, Mater. Sci. Eng. A 375–377 (2004) 213–218.
[7] J.-W. Yeh, S.-Y. Chang, Y.-D. Hong, S.-K. Chen, S.-J. Lin, Anomalous decrease in X-ray diffraction intensities of Cu–Ni–Al–Co–Cr–Fe–Si alloy systems with multi-principal elements, Mater. Chem. Phys. 103 (2007) 41–46.
[8] J.-W. Yeh et al., Nanostructured high-entropy alloys with multiple principal elements: novel alloy design concepts and outcomes, Adv. Eng. Mater. 6 (2004) 299–303.
[9] Y.Y. Chen, T. Duval, U.D. Hung, J.W. Yeh, H.C. Shih, Microstructure and electrochemical properties of high entropy alloys—a comparison with type-304 stainless steel, Corros. Sci. 47 (2005) 2257–2279.
[10] M.G. Poletti, G. Fiore, F. Gili, D. Mangherini, L. Battezzati, Development of a new high entropy alloy for wear resistance: FeCoCrNiW0.3 and FeCoCrNiW0.3 + 5 at.% of C, Mater. Des. 115 (2017) 247–254.
[11] Z.-S. Nong, Y.-N. Lei, J.-C. Zhu, Wear and oxidation resistances of AlCrFeNiTi-based high entropy alloys, Intermetallics 101 (2018) 144–151.
[12] B. Gludovatz et al., Exceptional damage-tolerance of a medium-entropy alloy CrCoNi at cryogenic temperatures, Nat. Commun. 7 (2016) 10602.
[13] C.-C. Juan et al., Enhanced mechanical properties of HfMoTaTiZr and HfMoNbTaTiZr refractory high-entropy alloys, Intermetallics 62 (2015) 76–83.
[14] O.N. Senkov, G.B. Wilks, J.M. Scott, D.B. Miracle, Mechanical properties of Nb25Mo25Ta25W25 and V20Nb20Mo20Ta20W20 refractory high entropy alloys, Intermetallics 19 (2011) 698–706.
[15] O. Maulik, D. Kumar, S. Kumar, S.K. Dewangan, V. Kumar, Structure and properties of lightweight high entropy alloys: a brief review, Mater. Res. Express 5 (2018).
[16] K.M. Youssef, A.J. Zaddach, C. Niu, D.L. Irving, C.C. Koch, A novel low-density, high-hardness, high-entropy alloy with close-packed single-phase nanocrystalline structures, Mater. Res. Lett. 3 (2015) 95–99.
[17] X. Yang, S.Y. Chen, J.D. Cotton, Y. Zhang, Phase stability of low-density, multiprincipal component alloys containing aluminum, magnesium, and lithium, JOM 66 (2014) 2009–2020.
[18] O. Maulik, D. Kumar, S. Kumar, D. M. Fabijanic, V. Kumar, Structural evolution of spark plasma sintered AlFeCuCrMgx (x = 0, 0.5, 1, 1.7) high entropy alloys. *Intermetallics* **77**, 2016 46–56
[19] R. Feng et al., Phase stability and transformation in a light-weight high-entropy alloy, Acta Mater. 146 (2018) 280–293.
[20] Y. Zhang et al., Microstructures and properties of high-entropy alloys, Prog. Mater. Sci. 61 (2014) 1–93.
[21] X. Yang, Y. Zhang, Prediction of high-entropy stabilized solid-solution in multi-component alloys, Mater. Chem. Phys. 132 (2012) 233–238.
[22] J.P. Perdew, Y. Wang, Accurate and simple analytic representation of the electron-gas correlation energy, Phys. Rev. B 45 (1992) 13244–13249.
[23] P.E. Blöchl, Projector augmented-wave method, Phys. Rev. B 50 (1994) 17953–17979.
[24] J.P. Perdew, K. Burke, Y. Wang, Generalized gradient approximation for the exchange-correlation hole of a many-electron system, Phys. Rev. B 54 (1996) 16533–16539.
[25] A.D. Becke, K.E. Edgecombe, A simple measure of electron localization in atomic and molecular systems, J. Chem. Phys. 92 (1990) 5397–5403.
[26] T.A. Manz, Introducing DDEC6 atomic population analysis: part 3. comprehensive method to compute bond orders, RSC Adv. 7 (2017) 45552–45581.
[27] R. Dronskowski, P.E. Blochl, Crystal Orbital Hamilton Populations (COHP): energy-resolved visualization of chemical bonding in solids based on density-functional calculations, J. Phys. Chem. 97 (1993) 8617–8624.
[28] A. Zunger, S.-H. Wei, L.G. Ferreira, J.E. Bernard, Special quasirandom structures, Phys. Rev. Lett. 65 (1990) 353–356.
[29] A. van de Walle et al., Efficient stochastic generation of special quasirandom structures, Calphad 42 (2013) 13–18.
[30] S. Guo, C.T. Liu, Phase stability in high entropy alloys: Formation of solid-solution phase or amorphous phase, Prog. Nat. Sci. Mater. Int. 21 (2011) 433–446.
[31] H. Heydari, M. Tajally, A. Habibolahzadeh, Calculations to introduce some light high entropy alloys based on phase formation rules, J. Alloys Compd. 912 (2022) 165222.
[32] H. Heydari, M. Tajally, A. Habibolahzadeh, Computational analysis of novel AlLiMgTiX light high entropy alloys, Mater. Chem. Phys. 280 (2022) 125834.
[33] J.B. Levine, S.H. Tolbert, R.B. Kaner, Advancements in the search for superhard ultra-incompressible metal borides, Adv. Funct. Mater. 19 (2009) 3519–3533.
[34] Y.L. Hu et al., First-principle calculation investigation of NbMoTaW based refractory high entropy alloys, J. Alloys Compd. 827 (2020) 153963.

[35] S. Qiu, N. Miao, J. Zhou, Z. Guo, Z. Sun, Strengthening mechanism of aluminum on elastic properties of NbVTiZr high-entropy alloys, Intermetallics 92 (2018) 7–14.
[36] S.-H. Jhi, J. Ihm, S.G. Louie, M.L. Cohen, Electronic mechanism of hardness enhancement in transition-metal carbonitrides, Nature 399 (1999) 132–134.
[37] S. F. Pugh, XCII. Relations between the elastic moduli and the plastic properties of polycrystalline pure metals. *London, Edinburgh, Dublin Philos. Mag. J. Sci.* **45**, 1954 823–843
[38] D.G. Pettifor, Theoretical predictions of structure and related properties of intermetallics, Mater. Sci. Technol. 8 (1992) 345–349.
[39] H.W. Yao et al., Mechanical properties of refractory high-entropy alloys: Experiments and modeling, J. Alloys Compd. 696 (2017) 1139–1150.
[40] Z. Rao et al., Machine learning–enabled high-entropy alloy discovery, Science (80-.) 378 (2022) 78–85.